2

REPORT DOCUMENTATION PAGE

Public reporting burden for this collection of information is estimated to average 1 hour per response, including the time for reviewing instructions, searching existing data sources, gathering and maintaining the data needed, and completing and reviewing the collection of information. Send comments regarding this burden estimate or any other aspect of this collection of information, including suggestions for reducing this burden, to Washington Headquarters Services, Directorate for Information Operations and Reports, 1215 Jefferson Davis Highway, Suite 1204, Arlington, VA 22202-4302, and to the Office of Management and Budget, Paperwork Reduction Project (0704-0188), Washington, DC 20503.

1. AGENCY USE ONLY (Leave blank)	2. REPORT DATE April 1995	3. REPORT TYPE AND DATES COVERED final 06/01/91 - 11/20/94

4. TITLE AND SUBTITLE	5. FUNDING NUMBERS
Free Stream Turbulence - A Unified Investigation of its Effects on Skin Friction and Heat Transfer	AFOSR 91-0295 (G)

6. AUTHOR(S)

Peter Bradshaw
Donald M. Bott

AFOSR TR
95-0647

DTIC
SELECTED
OCT 17 1995
S F D

7. PERFORMING ORGANIZATION NAME(S) AND ADDRESS(ES)	8. PERFORMING ORGANIZATION REPORT NUMBER
Mechanical Engineering Department Stanford University Stanford, CA 94305-3030	

9. SPONSORING/MONITORING AGENCY NAME(S) AND ADDRESS(ES)	10. SPONSORING/MONITORING AGENCY REPORT NUMBER
Air Force Office of Scientific Research 110 Duncan Avenue, Suite B115 Bolling AFB, DC 20332-0001 NA	AFOSR - 91-0295

11. SUPPLEMENTARY NOTES

19951013 036

12a. DISTRIBUTION/AVAILABILITY STATEMENT	TION CODE
Approved for public release; distribution unlimited	

13. ABSTRACT (Maximum 200 words)

Existing prediction formulas for the effect of free-stream turbulence (FST) on skin friction and heat transfer, based on measurements in low-intensity grid turbulence, fail at high intensities typical of the upstream stages of gas turbines. However, the previous evidence for this came from tests with various unconventional turbulence generators. In the present work measurements were made on the downstream-moving surface of a conveyor belt. This increased the effective value of Tu, the ratio of r.m.s. free-stream intensity to *the velocity difference across the boundary layer*. Thus conventional grids could be used to generate high Tu. Heat transfer was measured by a quasi-transient technique. A fixed heating lamp shone on the belt near its upstream end, and the streamwise decrease of surface temperature was measured using a chordwise strip of liquid crystals. Conductive heat transfer into the belt was calculable, so convective heat transfer into the airstream could be deduced. Skin-friction results collapse fairly well using Hancock & Bradshaw's combination of intensity and length scale but lie well above their low-Tu correlation.

DTIC QUALITY INSPECTED 5

14. SUBJECT TERMS		15. NUMBER OF PAGES 21
Free stream turbulence, heat transfer, gas turbines		16. PRICE CODE

17. SECURITY CLASSIFICATION OF REPORT UNCLASSIFIED	18. SECURITY CLASSIFICATION OF THIS PAGE UNCLASSIFIED	19. SECURITY CLASSIFICATION OF ABSTRACT UNCLASSIFIED	20. LIMITATION OF ABSTRACT UL

FINAL TECHNICAL REPORT ON AFOSR 91-0295
"Free Stream Turbulence – A Unified Investigation of Its Effects on Skin Friction and Heat Transfer"

1 June 1991 – 30 Nov. 1994

Peter Bradshaw, Principal Investigator
Donald M. Bott, Research Assistant

Mechanical Engineering Department
Stanford University, CA 94305
(415) 725-0704, Fax (415) 723-4548
e-mail bradshaw@stokes.stanford.edu

ABSTRACT

Existing prediction formulas for the effect of free-stream turbulence (FST) on skin friction and heat transfer, based on measurements in low-intensity grid turbulence, fail at high intensities typical of the upstream stages of gas turbines. However, the previous evidence for this came from tests with various unconventional turbulence generators. In the present work measurements were made on the downstream-moving surface of a conveyor belt. This increased the effective value of Tu, the ratio of r.m.s. free-stream intensity to *the velocity difference across the boundary layer*. Thus conventional grids could be used to generate high Tu. Heat transfer was measured by a quasi-transient technique. A fixed heating lamp shone on the belt near its upstream end, and the streamwise decrease of surface temperature was measured using a chordwise strip of liquid crystals. Conductive heat transfer into the belt was calculable, so convective heat transfer into the airstream could be deduced. Skin-friction results collapse fairly well using Hancock & Bradshaw's combination of intensity and length scale but lie well above their low-Tu correlation.

1. INTRODUCTION

Recent measurements, in several laboratories, of the effect of high-intensity turbulence on turbulent boundary layers in zero pressure gradient have shown larger increases in heat transfer and skin friction than would be predicted by plausible extrapolations of correlation formulas for data at low turbulence intensities. The implication is that these formulas seriously underestimate the heat transfer to first-stage blades in a gas turbine, directly downstream of the combustor. Accurate estimation of this heat transfer is vital: if it is underestimated in a real engine, blades creep or burn out; if it is overestimated, the turbine entry temperature will be chosen lower than need be, reducing engine efficiency.

The recent measurements (e.g. Refs. 1, 2) have been made with turbulence generators very different from the traditional square-mesh "biplane" grids of square or round bars, for which large quantities of experimental data are available and which produce turbulence

intensities of typically 5% to 10% of the mean velocity, whereas combustion chamber exit levels are of the order of 30% of the mean velocity. In some cases, the turbulence generator has been a plausible approximation to the flow in a combustor can (but without combustion as such). This undoubtedly increases assurance that the results should be applicable to real combustors, but the turbulence is usually spatially inhomogeneous and accompanied by significant variations of mean velocity, which directly affect boundary layer development and confuse the interpretation of free-stream-turbulence effects.

In the present project, a high effective turbulence level is obtained with ordinary grids, in the boundary layer on a downstream-moving belt forming the floor of a wind tunnel. Turbulence grids mounted upstream produce the customary turbulence levels with an r.m.s. value u' of 5% to 10% of the wind-tunnel speed. If the belt speed is U_b and the speed of the tunnel is U_∞, the velocity difference across the boundary layer is $U_\infty - U_b$ and the effective turbulence level – the ratio of r.m.s. turbulence level to this velocity difference – is $u'/(U_\infty - U_b)$. If $U_b = (2/3)U_\infty$ the effective turbulence level is therefore three times as large it would be on a stationary wall. The boundary layer on a moving wall is nearly but not exactly the same as that on a fixed wall: it can be thought of either as the boundary layer on a flat plate whose leading edge moves upstream at the (downstream) speed of the belt, or, more reassuringly, as a conventional boundary layer on a fixed surface with an unusually large velocity difference across the viscous sublayer. In this respect the boundary layer resembles that produced by polymer injection at the surface or by a hypothetical surface with "negative roughness".

2. EQUIPMENT AND TECHNIQUES

2.1. Wind Tunnel and Turbulence Grids

The measurements were made in the Mechanical Engineering Department's $30'' \times 30''$ low-speed blower tunnel (Figure 2.1: see also Schwarz & Bradshaw, Ref. 3). The maximum tunnel speed is about 27 m/s (90 ft/sec), and most measurements were made with the tunnel at near maximum speed, with belt speeds U_b from zero to the speed of the tunnel, the last situation being a repeat of the "shear-free turbulent boundary layer" with $U_b = U_\infty$, studied by Uzkan & Reynolds (Ref. 4) and Thomas & Hancock (Ref. 5).

The turbulence grid used for the main set of measurements had a biplane mesh of $1/2''$ square bars at $3''$ spacing, and was mounted, in a universal grid housing from which it could be easily removed, $22.5''$ upstream of the start of the moving floor.

2.2 Moving-Floor Rig

Construction of the moving floor (Fig. 2.2) follows standard technology for flat conveyor-belts (as distinct from the V-section ones used for carrying granular material). The – very helpful – suppliers of the belt asked what material we wished to convey: explanations were difficult.

The test section proper finishes at the end of the belt: the right-most of the three bays shown in Fig. 2.2 is left open.

Codes

Dist | Avail and / or Special

A-1

2

The two main rollers are slightly "crowned" (larger diameter at the middle than at the ends) to help keep the belt centered – exactly the same system was used for old-fashioned traction engine belting for driving threshing machines, which remained centered for length/width ratios approaching 100:1, even in the presence of pronounced vertical flapping. The middle 20 in. of the rollers is of constant diameter, 18 in., tapering to 17.96 in. at the ends. The upper surface of the belt is supported by a Teflon-coated plate over the rest of its length.

A temporary 1 HP drive motor was installed during the initial tests to help predict the power input required for high-speed running (finally a 5 HP (4kW) drive was installed, but the actual power absorption is the 3 HP, approx., estimated from the tests with the 1 HP motor: power is absorbed mainly by sliding friction forces between solid surfaces, which are roughly independent of speed).

The system worked very well and lining up of the roller axes in plan view proved to be straightforward. The smaller idler roller maintains belt tension: it is mounted on adjustment screws but is not spring-loaded. Thermal expansion of the belt was sufficiently small that the idler did not need adjustment for "hot" running.

We took, and have not regretted, the decision to assemble the test rig in the Department's workshop, using a flexible belt, a set of rollers, and a set of bearings, bought from specialist suppliers (see Table 1). Use of our own workshops, which have many other commitments, has probably meant a later delivery date than a commercial firm could offer, but has enabled us to consult with the machine shop staff at frequent intervals. This has produced a rig more closely suited to our requirements than could possibly be the case for a "turnkey" system of this unconventional kind bought from an external manufacturer .

We have had very little mechanical trouble with the system: also, contrary to our fears, we have not needed either active control of lateral wandering or suction to suppress vertical motion (both necessary in some moving-floor tunnels used for automotive testing).

We contemplated fitting sensors to shut down the motor if the belt wandered sideways enough for friction with the tunnel wall to be a problem, but short guides had to be fitted at the start of the flat portion of the belt surface to ensure that it could not be trapped where the drooped leading edge of the support plate joins the side walls, and these were enough to suppress wandering. The kinetic energy stored in the rollers at a belt speed of 100 ft/sec is nearly 200 HP-sec, so the 5HP motor took over half a minute to accelerate the belt and, conversely, any emergency shutdown method would work too slowly. A steel mesh deflector was placed at the end of the support framework (right-hand end of Fig. 2.2) to intercept the belt in case it broke and was extruded from the tunnel by the downstream drive roller, but we were assured by the suppliers that unheralded splice failures are very rare and none has occurred to date. The only belt damage has been caused by machining chippings trapped under the upstream fairing, leading to minor longitudinal scoring which was mechanically and aerodynamically negligible.

The only significant rig development work needed was concerned with sucking off the tunnel floor boundary layer upstream of the belt (Fig. 2.3). Without suction, the natural

tunnel boundary layer at the leading edge of the belt was 13 mm thick. The object is to remove all low-total-pressure air up to the leading edge of the belt. The difficulty is to maintain suction as close as possible to the cusped end of the upstream fairing while also maintaining structural integrity. A multi-slot arrangement was chosen in preference to a perforated plate, and has worked fairly well (Fig. 2.4). Another source of difficulty, also anticipated, is the flow induced by the return leg of the belt, which emerges at the front of the belt's upper surface as a "wall jet". This has been minimised by inserting a felt scrubbing strip between the fixed upstream fairing surface and the belt. A flexible strip (0.012 in steel shim) is used to minimise the step down from the fairing to the belt.

Despite these precautions, the momentum defect at the belt leading edge is acceptably small only for $U_b/U_\infty < 2/3$ (Fig. 2.5 shows the limiting case of $U_b/U_\infty = 1$). This operating range, implying an amplification factor of 3 for Tu, is adequate for present purposes: study of the limiting case would require an improved suction arrangement.

2.3 Velocity Measurements

Velocity measurements were made with standard pitot-tube and hot-wire techniques, the probes being mounted on a traverse gear (Ref. 3) extending from the roof of the tunnel. The constant-temperature hot-wire bridges used in the later stages of the work are described by Watmuff (Ref. 6), and the cross-wire probes are Dantec type **** (1 mm long, 5μm diameter tungsten wires). We anticipated having to leave a clearance of, say, $y = 0.02$ in. between the probe and the nominal surface position, to avoid contact if the belt flapped. In fact belt flapping was negligible and the main concern was aerodynamic interference due to the relative velocity between the probe and the surface.

Initially, the traverse gear happened to be fitted with a 3-hole yawmeter. In shakedown measurements of the velocity field over the moving belt with this device (using the central tube as a Pitot tube and obtaining static pressure from a separate surface tap on the tunnel sidewall) we found that readings within one or two tube diameters from the surface depended, in a consistent but puzzlingly nonlinear way, on the speed of the wall. Fig. 2.6 shows an example, a logarithmic plot of the velocity profile at a given x position, for different belt speeds. In these axes, all profiles should collapse for $y/\delta < 0.1 - 0.2$: the friction velocity u_τ was chosen to optimise collapse in the "log law" (straight-line) region, but the results for smaller y than this are obviously incorrect (results for $U_b = 0$ should of course be correct to normal measurement accuracy). These discrepancies are certainly not caused by inaccuracies in determining the distance of the probe from the wall or in measuring the belt speed (which would not be so consistent), although the latter sources of error are a complicating factor. Clearly the belt induces a velocity relative to the probe which would not be present on a fixed wall, but this is not an explanation of why the yawmeter reads the *wrong* velocity. When the probe is close to the surface, the flow induced by the belt has to pass over, or to the side of, the probe: so that the basic effect is probably an upflow over the front of the tube, causing a displacement of the effective center. A single Pitot tube showed much smaller effects, and the log-law plots presented in Section 3 are universal down to the smallest value of y, independent of belt speed. Therefore we did not explore the interference phenomenon in any detail.

4

We had not anticipated that any moving-wall interference would be significant with the yawmeter so far from the surface. However we were not surprised that the shear stress indicated by a Preston tube (a Pitot tube *touching* the surface) disagrees quite strongly with that obtained from the logarithmic law because of the same moving-wall interference: a Preston-tube calibration with U_b/u_τ as an additional parameter could be deduced from the log-law skin friction but there is no point in doing this in the present experiment. Hot-wire probes seem to be much less subject to moving-wall interference, but calibration drift due to fluid temperature changes make them unattractive for mean velocity measurement.

The interference could presumably be correlated according to law-of-the-wall principles as $\Delta U/u_\tau = f(U_b/u_\tau, y/d, u_\tau d/\nu)$ or, for a Preston tube, as $\Delta \tau_w/\tau_w = f(U_b/u_\tau, u_\tau d/\nu)$, but we did not attempt to do this because the case of a probe close to a surface moving exactly downstream is rare in practice. Also of course it would be unwise to bring a Pitot tube in rubbing contact with the surface.

In the present situation the only additional uncertainties in deducing surface shear stress from a logarithmic-law fit to the velocity profile near the surface (but outside the range of any probe interference) are the slight extra difficulty of determining the distance of the probe from the surface, and the fact that the velocity relative to the surface is actually the small difference of independently-measured large quantities. The results presented below are for $U_b/U_\infty \le 2/3$ so the ill-conditioning is not serious (though random scatter in the plots of quantities normalised by $U_\infty - U_b$ becomes noticeable as that velocity difference decreases, the absolute velocity scatter in meters/sec being roughly independent of belt speed).

2.4 Heat-Transfer Measurements

The technique used to measure heat transfer was finalised fairly late in the project, because there were several contenders including the rapidly-developing technique of infra-red imaging. The fallback option was a heat balance for a control volume whose upper surface was coincident with the upper surface of the tunnel floor belt and which enclosed an electrical heater and also the belt drive motor (whose electrical input was known). We finally developed a variation of the transient technique of Hacker & Eaton (Ref. 7). Their procedure is to move a time-dependent heat source (an electric lamp) slowly over a stationary surface (a thin metal sheet on an insulated substrate) to generate any desired surface-temperature distribution $T_w(x)$, and then start the flow so that convective heat transfer rates can be deduced from the rate of cooling of the sheet, itself deduced from $T_w(x,t)$, deduced in turn from color changes in a layer of cholesteric liquid crystals, if necessary with an allowance for radiation. Here we heat the moving surface with a constant, fixed light source and observe $T_w(x)$ using crystals painted on the belt surface. This is equivalent to the Hacker-Eaton technique for the case of a short pulse of heat of duration $\Delta x/U_b$ where Δx is the spatial extent of the heated region.

We need to measure the difference between the heat transfer from the moving belt *with* heating and the heat transfer (due to drive friction) *without* heating, and in both cases an allowance for radiation must be made. Fortunately, heat transfer with small temperature

differences is linear and we are interested only in the *percentage* increase in convective heat transfer due to free-stream turbulence. Also, the unheated belt is only 1 to 3 deg. C above air temperature. Therefore the technique is relatively well conditioned.

Our justification for using small temperature differences is that heat-transfer prediction methods developed in constant-property flows seem to suffice at least up to moderate supersonic speeds and for wall-to-free-stream temperature ratios up to three or more, and there is no reason to suppose that the effect of FST and large temperature difference interact. Therefore, constant-property data should be adequate for testing prediction methods for FST and/or large temperature differences.

The crystal-bearing "paint" adhered satisfactorily to the synthetic rubber belt surface in spite of the flexing of the latter as it moved over the rollers, and we saw no evidence of degradation. This removes the most serious question concerning the use of the technique. Another question is uniformity of thickness of the crystal layer. The finite response time of the crystals is due to heat conduction through the layer (about 40–50 μm thick) rather than to the crystal reaction time as such, and – given an estimate of the conductivity k and the specific heat c – can be allowed for as part of the process of deducing heat transfer rate from rate of change of indicated surface temperature.

Our available heat source is a 1kW halogen photographic lamp (or an array thereof): it is mounted in the suction chamber at the upstream end of the belt (Fig. 2.3: the inset describes the limited temperature range over which the crystals change color) and the support arrangements are shown in Fig. 2.7. The length of the bulb (in the spanwise direction) is many times the thickness of the belt so that spanwise heat transfer can be ignored. An alternative would be to use a point source, provided by a high-powered laser mounted outside the tunnel, but this would involve several difficulties.

The present state is that the software for conduction caluations has been written, the system is working and the resolution appears to be adequate, but final video images have not yet been taken. The image processing system has been thoroughly checked out by Hacker & Eaton and other workers in the group.

2.5 Turbulence Grid

Detailed measurements have been taken with only one grid, with a 3 in. mesh of 1/2 in. bars. Fig. 2.8 shows the decay of all three components of intensity, and Fig. 2.9 the growth of length scale L_e, defined (Ref. 8) in terms of u-component decay alone so that for isotropic turbulence it would be $(2/3)^{1/2} k^{3/2}/\epsilon$. In these two figures only, x is measured from the grid rather than the start of the moving surface. Fig. 2.10 shows the parameter space covered in the detailed measurements presented below (here Tu is the effective value based on $U_\infty - U_b$). As pointed out in Ref. 8, it is difficult to cover a wide region in this space: in the present arrangement, increasing belt speed increases effective Tu but also increases L_e/δ because δ decreases.

3. RESULTS WITHOUT TURBULENCE GRID

The results are normalized by velocity difference and plotted against y as such, to show the way the profiles change with floor speed: optimum collapse of data would be obtained by scaling with u_τ and δ. The main purpose of presenting the results is to show that, as argued at the end of Section 1, the moving-floor boundary layer is not essentially different from a conventional one, either for fundamental reasons or because of imperfections in the present apparatus. Fig. 3.* shows comparisons of skin-friction coefficient, deduced from the log-law plots, with a simple formula for conventional boundary layers in zero pressure gradient, $c_f = 0.025[(U_\infty - U_b)\theta/\nu]^{-1/4}]$ (Ref. 9: this formula is about 5% lower than the implicit formula of Coles). The measurements are lower than the formula by a small but consistent amount, probably within the range of likely accuracy of the "Clauser chart" technique. There is no detectable trend with belt speed ratio, indicating that, at lest in this important respect, the moving-belt boundary layer has the same properties as a conventional flat plate boundary layer although of course its rate of growth seen by a stationary observer is lower. This bears out the more qualitative impression that the velocity profiles are entirely normal.

4. RESULTS WITH TURBULENCE GRID

Analysis of the results is still in progress: here they are presented without detailed discussion. Sufficient detail (including measurements of triple products) is available for budgets of each of the Reynolds stresses to be evaluated (with plausible assumptions). A summary of the results is provided by the skin-friction values, deduced on the assumption that the logarithmic law of the wall applies even at high FST. Bradshaw & Huang (Ref. 10) have pointed out that the fragility of the temperature law of the wall (which is not relied on in the present work) casts doubt on the velocity law of the wall, which depends on closely analogous similarity arguments. However, the velocity profiles in the present measurements seem to follow the law of the wall satisfactorily over extended regions, whereas one would expect any perturbations caused by FST to be strongly dependent on y because of the effect of the impermeable wall constraint, which causes large y-wise gradients in FST intensity over the whole range $0 < y < L_e$.

The increments in skin friction are plotted in Figs. 4.*–4.*, first against Tu alone, then against the parameter recommended by Hancock & Bradshaw, and finally against that parameter as modified for low-Reynolds-number effects by Blair (Ref. 11) and Castro (Ref. 12). Disconcertingly, the scatter is slightly smaller in the plot against Tu than in the plots using the more refined parameters. However the values at low Tu agree fairly well with Hancock & Bradshaw's correlation, though they rise well above it at high values of Hancock & Bradshaw's parameter. Even a linear fit to the low-intensity part of the correlation would underestimate the present results.

5. CONCLUSIONS

The work described here has used a novel technique to produce high effective intensities of FST from conventional turbulence grids, avoiding the uncertainties associated with the unconventional generators of high FST reported in the literature, which produce inhomogeneities of mean flow and turbulence. The main conclusion is that even grid turbulence produces larger increases in skin-friction coefficient c_f at high FST than are predicted by plausible extrapolations of fits to low-FST data – the magnitude of the discrepancy depending on whether the extrapolations assume a linear relation between c_f and r.m.s. FST, or a more sophisticated formula like that of Hancock & Bradshaw (Ref. 8). This does not necessarily validate the quantitative results obtained with unconventional generators, but implies that they are not qualitatively misleading.

The work is continuing, unfunded. Further analysis is in progress and final heat transfer measurements are about to be taken. A PhD thesis is in preparation.

6. AKNOWLEDGEMENTS

7. REFERENCES

1. Young, C.D., Han, J.C., Huang, Y. and Rivir, R.B. Influence of jet-grid turbulence on flat plate turbulent boundary layer flow and heat transfer. J. Heat Transfer **114**, 65, 1992.

2. Ames, F.E., and Moffat, R.J. Heat transfer with high intensity large scale turbulence: the flat plate boundary layer and the cylindrical stagnation point. Stanford University Rept HMT-44, 1990.

3. Schwarz, W.R. and Bradshaw, P. Three-dimensional turbulent boundary layer in a 30 degree bend – experiment and modeling. Stanford Univ. Mech Engg Dept Rept MD-61, 1992.

4. Uzkan, T., and Reynolds, W.C. A shear-free turbulent boundary layer. J. Fluid Mech. **28**, 803, 1967.

5. Thomas, N.H. and Hancock, P.E. Grid turbulence near a moving wall. J. Fluid Mech. **82**, 481, 1977.

6. Watmuff, J.H. A high-performance constant-temperature hot-wire anemometer. NASA CR 177645, 1994.

7. Hacker, J. and Eaton, J.K. A heat transfer measurement technique which allows arbitrary wall temperature distributions. ASME HTD **206-1**, 71 (Keyhani et al., eds.),

1992.

8. Hancock, P.E., and Bradshaw, P. Turbulence structure of a boundary layer beneath a turbulent free stream. J. Fluid Mech. **205**, 45, 1989.

9. Kays, W.M. and Crawford, M.E. *Convective Heat and Mass Transfer* (3rd. Ed.). McGraw-Hill (1993).

10. Bradshaw, P. and Huang, P.G. The law of the wall in turbulent flow. Presented at Osborne Reynolds Centenary Symposium, Manchester, 1994; to appear in Proc. Roy. Soc. London, 1995.

11. Blair, M.F. Influence of free stream turbulence on turbulent boundary layer heat transfer and mean profile development. Parts I and II. J. Heat Transf. **105**, 33 and 41, 1983.

12. Castro, I.P. Effects of free stream turbulence on low Reynolds number boundary layers. J. Fluids Engg. **106**, 298, 1984.

7. PROFESSIONAL PERSONNEL

Prof. Peter Bradshaw, Principal Investigator.

R. Matthew Ohline, M.S. student, June-August 1991.

Donald M. Bott, Ph.D. student, September 1991-present.

TABLE 1 – SUPPLIERS AND SPECIFICATIONS

Belt (Bay Belting Services, Ammeraal Group, 5637 La Ribera St, Ste A, Livermore CA 94550). 30″ wide, 20′ long, 2 mm thick rubberized fabric.

Crowned rollers 18″ dia., 32″ long, ends tapered 0.02″ on radius starting 6.4″ from each end: friction-drive roller coated with 3/8″ neoprene lagging. Balanced to 1300 rpm.

Idler (tensioning) roller 6″ dia., length and taper as for main rollers.

Bearings (Kaman Industrial Technologies) Dodge K/DI 2-3/16″ pillow block type

Drive motor Eaton Dynamatic 5 HP eddy current drive
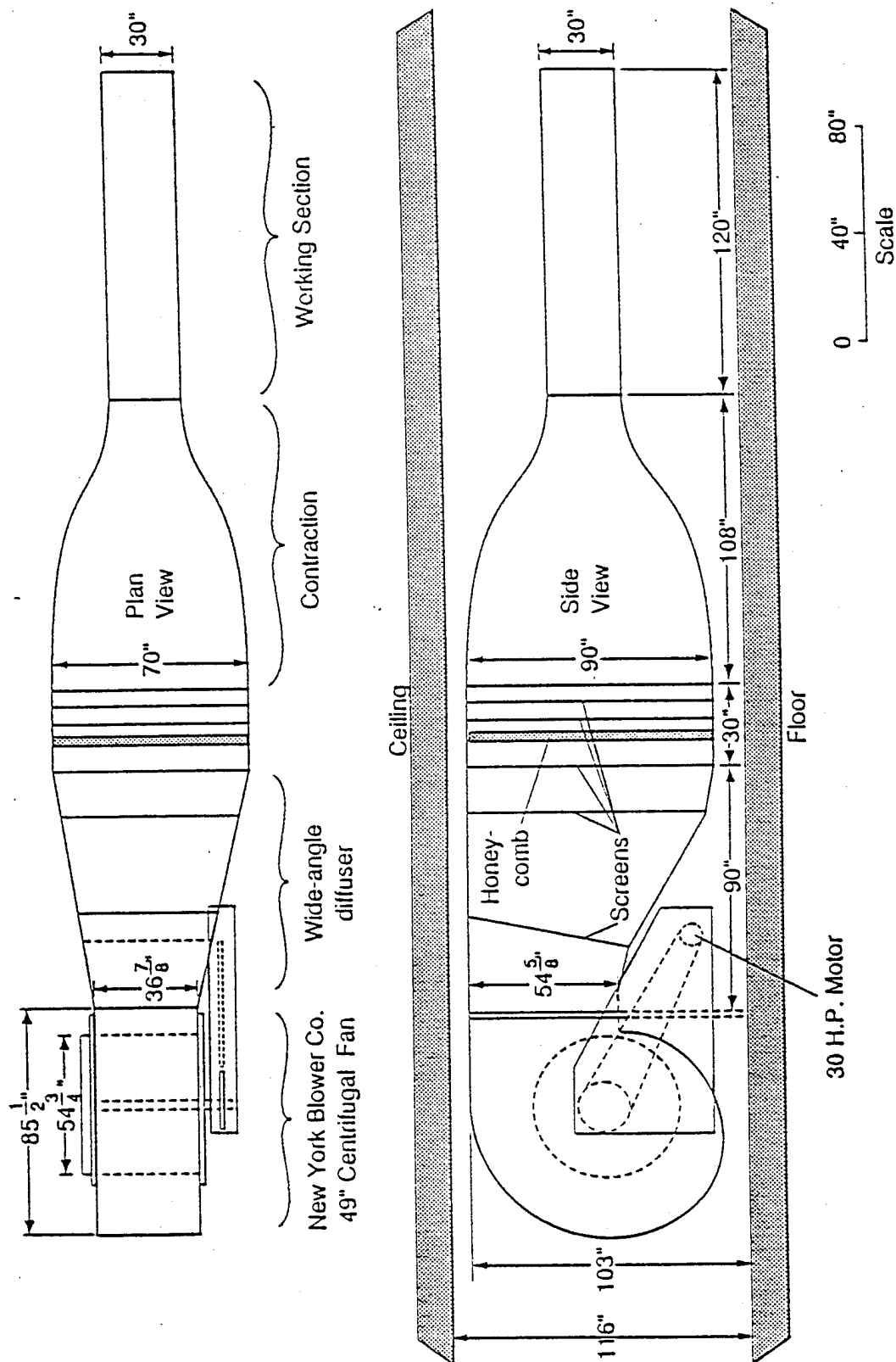
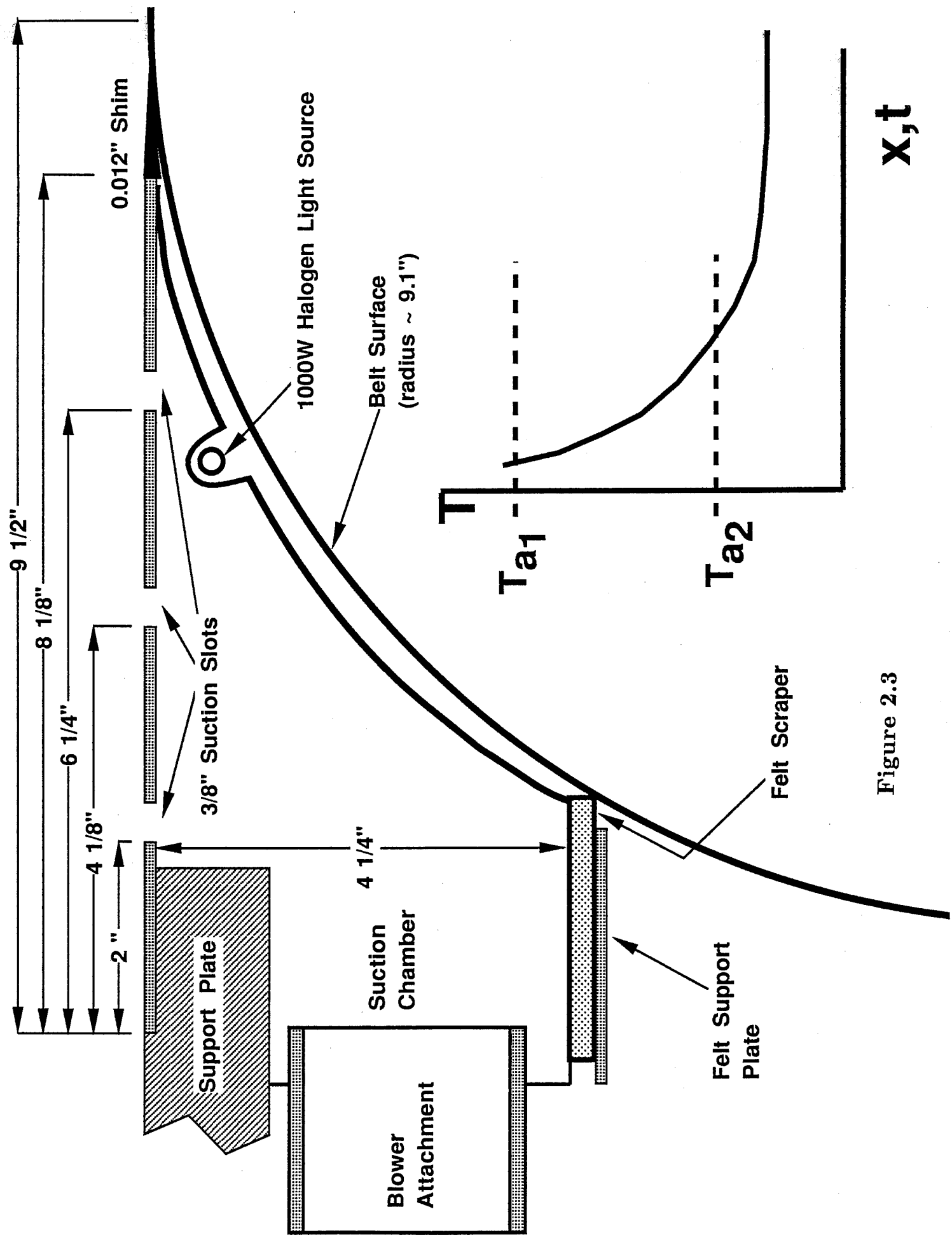**Figure 2.1** 30" by 30" blower tunnel

Moving–Wall Test Section

Maximum belt speed: >30 m/s

6'8"

15'2"

7'8"

Teflon–coated
backing plate

18" lagged
drive roller

5 hp. eddy–
current drive

6" Idler roller

18" driven roller

Suction slots

30" x30"
tunnel

Suction
blower

Figure 2.2

0.012" Shim

9 1/2"

8 1/8"

6 1/4"

4 1/8"

2 "

1000W Halogen Light Source

Belt Surface
(radius ~ 9.1")

3/8" Suction Slots

Support Plate

4 1/4"

Suction
Chamber

Blower
Attachment

Felt Support
Plate

Felt Scraper

T

T_{a1}

T_{a2}

x,t

Figure 2.3

Effect of suction on inlet boundary layer

Legend:
- With suction--mid slot
- Without suction
- With suction--5 mm from slot end

U [m/s] (vertical axis): 25, 20, 15, 10

y [m] (horizontal axis): 0.01, 0.02, 0.03

Figure 2.4

Figure 2.5

Figure 2.6

Power Lead

Leading Edge Support

1/4" Threaded Steel Electrode

Stainless Lamp Support Collar

Wiko® FCM 1000W Halogen Lamp

Cutaway to show electrode location

2.4"

4.6"

Figure 2.7

Figure 2.8

Figure 2.9

L/δ vs Tu Parameter Space

Figure 2.10